Buoyancy of Convective Clouds in TOGA COARE

DINGYING WEI, ALAN M. BLYTH, AND DAVID J. RAYMOND

Department of Physics and Geophysical Research Center, New Mexico Institute of Mining and Technology, Socorro, New Mexico

(Manuscript received 5 May 1997, in final form 23 January 1998)

ABSTRACT

The buoyancy of convective clouds in TOGA COARE was calculated from the NCAR Electra in situ measurements of temperature, humidity, liquid water content, and two-dimensional images of raindrops. Most of the measurements were made at 700 mb (10°C) although some were made at 850 (18°C) and 600 mb (2°C). The temperature was measured with the Ophir radiometer, which does not have the wetting problem that has degraded many previous measurements of in-cloud temperature in warm clouds.

On average, the in-cloud virtual temperature excess was found to be less than the adiabatic value by about 2 K, while the negative influence of total water content on buoyancy was less than 0.5 K. Furthermore, the total water content was highly variable and much smaller than the adiabatic value. The authors conclude, therefore, that entrainment and mixing was usually a much larger factor in reducing the buoyancy than water loading.

The average buoyancy in downdrafts was positive and similar to the value in updrafts.

1. Introduction

One of the surprising results of the Global Atmospheric Research Program's Atlantic Tropical Experiment (GATE) was that updrafts were observed to be weaker than those in the Thunderstorm Project (LeMone and Zipser 1980; Zipser and LeMone 1980; Byers and Braham 1949). Observations made by Barnes et al. (1983), Jorgensen et al. (1985), Jorgensen and LeMone (1989), Lucas et al. (1994a,b), and others further confirmed that convective updrafts over tropical and subtropical oceans are weaker than convective updrafts in continental storms.

Zipser and LeMone (1980) and Jorgensen et al. (1985) noticed that the measured updraft velocity in clouds over the ocean was only a small fraction of what was expected from parcel theory. Jorgensen and LeMone (1989, hereafter JL) calculated cloud buoyancy using the temperature measured with a CO_2 radiometric thermometer and concluded that both water loading and entrainment played a significant role in reducing buoyancy and vertical velocity in updrafts. They also found that the majority of the strongest downdrafts were warmer than the environment.

Recently, Lucas et al. (1994a, hereafter LZL) examined the data obtained during the Equatorial Mesoscale Experiment that took place in the Gulf of Carpentaria north of Australia. They speculated that water loading is more effective in reducing buoyancy in oceanic convection than in continental convection because the lifted parcel's virtual temperature excess in soundings over tropical oceans is smaller. They also speculated that entrainment is more effective in reducing buoyancy in oceanic convection because the thermal cores are smaller.

In this paper, we examine the buoyancy of cumulus convection that occurred in the western equatorial Pacific using temperature measured by the Ophir III radiometer and precipitation water content measured by the Particle Measuring System (PMS) 2D probes (Knollenberg 1981). The measurements were gathered during the Tropical Ocean and Global Atmosphere Coupled Ocean–Atmosphere Response Experiment (TOGA COARE) (Webster and Lucas 1992) using the National Center for Atmospheric Research (NCAR) Electra. The cloud regions penetrated were typically part of large systems tens of kilometers across, often reaching an altitude of 15 km or higher. The flight plans were such that long penetrations were made through the system, so flights were just as likely to encounter stratiform regions of cloud as convective regions. The aircraft did not make many penetrations through precipitation-free turrets. In fact precipitation was often encountered during the first penetration. Typical values of cloud base pressure and temperature were $p = 940$ mb, $T = 23$°C; that is, about 600 m above mean sea level. Penetrations were made by the Electra at $p \approx 600$, 700, and 850 mb ($T \approx 2°$, 10°, and 18°C). Table 1 shows the flights chosen for this study. The boundary layer missions were not included since only a few cloud penetrations were made. Flight 30 was not included since the aircraft did not

Corresponding author address: Alan Blyth, Department of Physics, New Mexico Institute of Mining and Technology, Socorro, NM 87801.
E-mail: blyth@kestrel.nmt.edu

TABLE 1. Flight number, date, and penetration levels of the flights analyzed in this study. Notice that penetrations were made at only one level in most flights.

Flight no.	Date	Penetration levels (mb)
02	19 Nov 92	600, 700
07	5 Dec 92	850
08	6 Dec 92	850
13	13 Dec 92	850
14	14 Dec 92	700
15	15 Dec 92	700
18	12 Jan 93	850
25	27 Jan 93	700
27	4 Feb 93	700
28	6 Feb 93	700
29	9 Feb 93	700
31	17 Feb 93	850, 550
32	18 Feb 93	850, 700

encounter very much clear air so it was difficult to process the temperature measurements.

2. Analysis methods

We define cloud buoyancy B as

$$B \equiv \Delta T_v - B_l, \tag{1}$$

where $\Delta T_v = T_v - T_{ve}$ and $B_l = T_{ve} r_l$. Here, T_v and T_{ve} are, respectively, the virtual temperature in cloud and in the environment, and r_l is the total liquid water mixing ratio. The in situ measurements of temperature, pressure, cloud water content, and PMS data were used. All data were averaged to 1 Hz by NCAR. The King probe was used for cloud water mixing ratio, although the Johnson–Williams probe was used when the King probe was not working. The precipitation water mixing ratio was calculated from the PMS probes.

In the results presented in section 4, we do not limit the analysis to updraft and downdraft cores in the manner described by LZL, for example. Instead, we consider a region to be an updraft or downdraft if the vertical wind speed, $w > 1$ m s^{-1} and $w < -1$ m s^{-1}, respectively. We further limit the analysis to regions with cloud liquid water content (LWC) measured by the forward-scattering spectometer probe (FSSP) greater than 0.03 g m^{-3}.

a. Temperature

Accurate in-cloud temperature measurements are crucial for determining cloud buoyancy. Measurement of in-cloud temperature is usually made by sensors that are immersed in air. The temperature measured in this manner has been determined to be too low in clouds where $T \geq -2$°C due to wetting of the sensor (Lenschow and Pennell 1974; Heymsfield et al. 1979; LeMone 1980; Cooper 1987; Lawson and Rodi 1987; Blyth et al. 1988; Lawson and Cooper 1990). The evaporative cooling caused by the wetting problem in warm clouds is typically 1–3 K, which is comparable to the magnitude of cloud buoyancy (Lawson 1990). Moreover, it is impossible to make any corrections for the effect of wetting since it is difficult to determine how much of the sensor is wet.

The first results using an airborne radiometric thermometer showed that the in-cloud heat flux was more than four times greater than that from Rosemount measurements, and it was in good agreement with the numerical simulation (Albrecht et al. 1979). Jorgensen and LeMone (1985) found, using a CO_2 radiometer, that the majority of the updraft cores had positive temperature anomalies in warm oceanic convective clouds as expected, and Lawson (1990) found that the Ophir radiometric measurements made in adiabatic cores of warm clouds were in good agreement with the calculated values. Furthermore, Cooper (1987) concluded that the Ophir measurements agreed well with the temperature measured by immersed sensors in clear air and that the Ophir was not affected by the wetting inside of clouds.

The Ophir radiometer used in this study senses the spectral radiance at a wavelength of 4.25 μm rather than at 15 μm, which was used in other radiometers in previous experiments (Albrecht et al. 1979; JL; LZL). CO_2 is a stronger absorber and emitter at 4.25 than at 15 μm. Therefore, the sample volume of the 4.25 μm radiometer is smaller. Moreover, absorption and emission by liquid water at 4.25 μm is weaker than at 15 μm, so the measurements of the 4.25-μm radiometer are less affected by water drops. A 4.25-μm radiometer receives significant radiation from cloud droplets only in very dense clouds where the difference between the droplet temperature and air temperature is believed to be smaller than 0.1 K (Lawson and Cooper 1990). On the other hand, temperature measurements made by a 15-μm radiometer can be too low in subsaturated cloud regions where water drops can be as much as 1 K colder than the air (Jorgensen and LeMone 1989).

The calibration of the Ophir probe was based on the finding that the Ophir radiometer behaves in the same manner inside a cloud as in clear air and the belief that the temperature measured by immersion sensors is reliable in clear air (Lawson and Cooper 1990). The temperature measured by the Rosemount probe ($T_{\rm ros}$) in clear air was used as a base line for the Ophir data to remove the offset.

The calibration involves five steps. The first step was to linearly interpolate $T_{\rm ros}$ between two points before and after a cloud to remove the wetting effect on the base temperature. Since it usually takes about 10 s for immersed sensors to dry out, the interpolation is carried out from the clear region 20 s before entering a cloud to the clear region 20 s after exiting the cloud. A cloud is defined as the region where cloud LWC measured by FSSP probe is greater than 0.03 g m^{-3}.

The second step was to obtain the low-frequency part of $T_{\rm ros}$ processed in the previous step. The low-pass filter used here consists of both a forward and backward filter

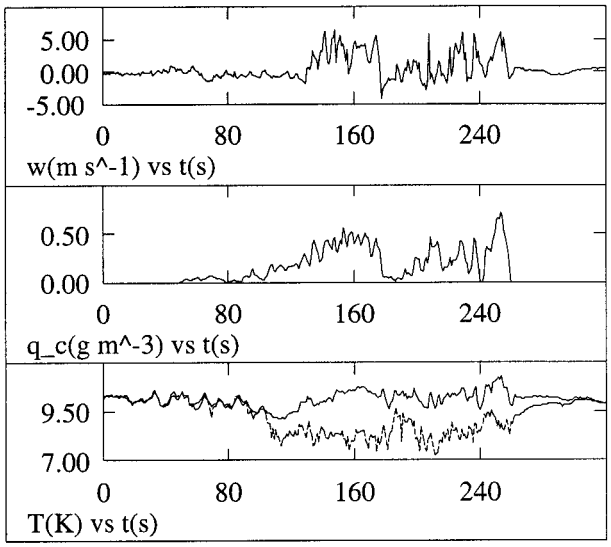

FIG. 1. Data from the cloud penetration at 1909:20 UTC on 14 December 1992 plotted versus time in seconds. Here, 1 s corresponds to about 100 m. From top to bottom panel: vertical air velocity (w) in m s^{-1}, cloud liquid water content (q_c) in g m^{-3}, and temperature measurements (T) in °C from the Rosemount (dashed, lower line) and corrected Ophir (solid line).

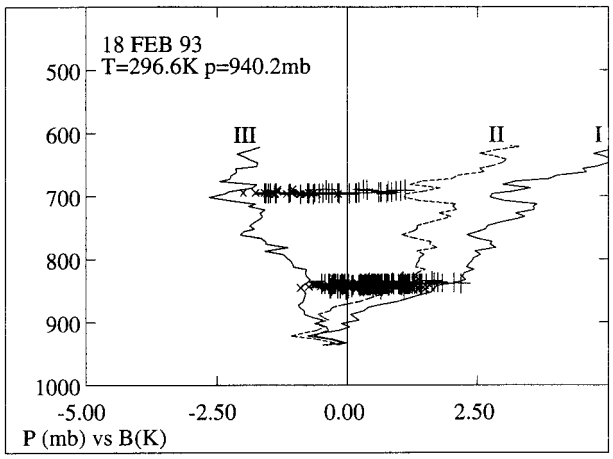

FIG. 2. Values of ΔT_v and B versus pressure for a sounding taken at 0220 UTC 19 February 1993 (18 February case). Curve I is the virtual temperature excess (ΔT_v) in a parcel lifted adiabatically from cloud base. Curve II is the buoyancy with all the condensed water in the parcel. Curve III is the minimum value of ΔT_v after all the liquid has been evaporated. The points correspond to in-cloud measurements of ΔT_v in cloud regions with no particles larger than 800-μm diameter: plus signs, $w > 1$ m s^{-1}; crosses, $w < -1$ m s^{-1}.

so that there is no phase shift in the filtered data. The forward filter is

$$x'_i = 0.99x'_{i-1} + 0.01x_i, \quad \text{and} \quad x'_0 = x_0,$$

where $i = 1, 2, \ldots, N-1$; $x_0, x_1, \ldots, x_{N-1}$ are the input data, and $x'_0, x'_1, \ldots, x'_{N-1}$ are the forward-filtered data. The backward filter is

$$x''_i = 0.99x''_{i+1} + 0.01x'_i, \quad \text{and} \quad x'_{N-1} = x'_{N-1},$$

where $i = N-1, N-2, \ldots, 2, 1, 0$; and $x''_0, x''_1, \ldots, x''_{N-1}$ are the low-pass filtered data. The low-pass filter has a cutoff frequency of 1.59×10^{-3} Hz, which is about 60 km at 100 m s^{-1} true airspeed.

The third step was to obtain the high-frequency components of the Ophir signal by subtracting the low-frequency components from the raw data.

The fourth step was to de-spike the Ophir temperature, T_{oph}. If the high-frequency component of T_{oph} was greater than a threshold value of 0.8 K, the Ophir measurements in that time period were treated as a spike, and a linear interpolation was performed. The threshold value was determined by examining the data.

The final step was to combine the low-frequency part of T_{ros} obtained in the second step with the scaled, de-spiked high-frequency component of T_{oph} to produce the final temperature T_c. A scaling factor was used to adjust the magnitude of the variations in the high-frequency part of T_{oph}. It was determined by comparing the high-frequency components of T_{oph} with those of T_{ros} filtered by the same filter in clear air.

Figure 1 shows an example of the behavior of the corrected Ophir temperature T_c and the Rosemount temperature T_{ros} on 14 December 1992. The effect of wetting on the Rosemount is clearly seen: T_{ros} decreased significantly upon entering the cloud and then required about 10 s to dry after exiting the cloud. Here, T_c is greater in the cloud region. Notice that the difference $T_c - T_{\text{ros}}$ is greater in regions with larger cloud liquid water, q_c. The match of T_c and T_{ros} in the clear air away from the cloud is by design of the correction procedure.

Figure 2 shows that T_{oph} values are within the limits predicted from parcel theory. The line on the negative side of the figure is the virtual temperature expected if all of the adiabatic liquid water is evaporated by mixing with the environmental air at the given altitude, while the line on the positive side is that expected in an adiabatic parcel. The Electra sounding taken at 0220 UTC on 19 February was used with a value of cloud base ($p = 940.2$ mb, $T = 23.4$°C) determined from flight legs flown beneath the cloud.

The environmental temperature used in the analysis was calculated in the clear regions 20 s of flight time away from and on both sides of the cloud. Since clear air that is near convection might be stabilized (destabilized) by low-level mesoscale sinking (lifting) (JL), the environmental temperature might have been modified by convection when there were not enough clear regions between cloud penetrations. The buoyancy calculated here is the buoyancy relative to the adjacent environment of convective clouds rather than relative to the unmodified environment.

b. Humidity

The NCAR Electra was equipped with a Lyman-alpha and UV hygrometer as well as the standard chilled mir-

ror device. The chilled mirror instrument provides reliable humidity measurements in clear air, but it has a slow response. The Lyman-alpha and UV hygrometer have a faster response time and better resolution but have calibration drift problems. Humidity values were constructed in this analysis from the low-frequency signal from the chilled mirror device combined with the high-frequency component of the signal from the Lyman-alpha. The UV hygrometer was used when the Lyman-alpha was not working.

The mixing ratio was assumed to be saturated inside clouds. The error in buoyancy resulting from this assumption is smaller than 0.1 K in cumulus clouds since the maximum supersaturation is usually smaller than 0.5% (Politovich and Cooper 1988). However, the error can be larger if a cloud is actually subsaturated. When the saturation assumption is used, an error of 1 g kg^{-1} in vapor mixing ratio will cause an error of 0.2 K in buoyancy.

c. The precipitation water content

Precipitation water content was obtained by integrating the masses of all particles measured by the PMS two-dimensional optical array probes. The probes were located in front of the wingtips, so that the measurements were not disturbed by flow over the fuselage of the aircraft. The probes produce two-dimensional images of particles with diameters ranging from about 100 μm to 6.4 mm, or larger with proper reconstruction of partial captured images (Heymsfield and Parrish 1979).

The image of a particle is taken in slices: the slice rate is adjusted so that the resolution along the flight direction is equivalent to that along the direction of orientation of the photodiodes. The maximum rate at which the 2D probe can store image slices is 4×10^6 slices per second (Baumgardner 1989). The high sampling rate can cause an overflow in the data acquisition system, which results in the probe ceasing to take data.

The equivalent size of a particle can be derived from its two-dimensional image by proper curve fitting. However, this process is complicated by two factors: 1) many particles are only partially imaged, and 2) large drops are generally elliptical in shape and canted forward. The shapes of falling liquid drops are strongly dependent on their sizes due to aerodynamic forces. Precipitation particles with diameters larger than about 200 μm are usually deformed into approximate oblate spheroids that are flattened at the bottom and round at the top (Magono 1954; Pruppacher and Beard 1970; Cooper et al. 1983). The accelerated airflow ahead of the probe was thought to be the cause of the canting (Beard and Jameson 1983; Beard 1983). However, Chandrasekar et al. (1988) found that the canting mainly results from the fall of drops as they pass through the aperture of the probe. The angle is dependent on the ratio of the minor axis to the major axis of the drop and the ratio of the fall speed of the drop relative to the speed of the aircraft.

We included the effect of canting and the nonspherical shape of the images in the 2D processing. Both elliptical and spherical curve fitting were used to determine the size of particles. The volume equivalent size was taken as the particle size. When the image was a whole particle, an elliptical fit was used. Otherwise a spherical fit was used for simplicity. For partially imaged particles, the fraction of the imaged particle was counted so that the sample volume was not affected. If we count the whole particle, then we have to adjust the sample volume since part of the particle is actually out of the sample volume of the instrument for that size of particle. Only those particles in which at least a half of the particle was imaged were taken into account. The following images were rejected in the calculation: images of less than half a particle, images with holes and many segments, and images whose one dimension is more than four times longer than the other dimension.

The calculation of concentration for one of the 2D probes was complicated by the frequent omission of the time bar following the timing word. The difficulty was largely alleviated by counting the number of transitions between on and off bits in each word to distinguish between a particle and a timing word.

d. The subcloud air

The magnitude of the variations in the reversible equivalent potential temperature θ_e entering the cloud is important since we compare, in the next section, the adiabatic value of ΔT_v with the in-cloud values. Large variations in boundary layer θ_e, such as reported by Raymond (1995), are usually associated with downdrafts. Figure 3 shows values of θ_e measured during a leg flown under cloud base on 5 December 1992. We can see that in any one precipitation-free updraft, values of θ_e varied by no more than 0.5 K. However, θ_e varied by about 1.5 K from one updraft to the next since θ_e varies on the mesoscale. This corresponds to a difference in ΔT_v for an adiabatic parcel ascending from cloud base to 700 mb of about 0.7 K. As we shall see, this is smaller than the difference between an average adiabatic value and the measured values.

3. Results

The 1-Hz buoyancy values were calculated from in situ temperature, humidity, cloud liquid water content, and precipitation water content measurements using Eq. (1). The buoyancy varied in the 13 cloud systems studied from -2.4 to 3.3 K with an overall average of about zero. The in-cloud temperature excess (ΔT_v) ranged from -2.3 to 3.4 K and the maximum negative buoyancy from liquid water loading was 2.5 K.

In this section, we present the averages of B, ΔT_v, and B_l in updrafts and downdrafts at the three different levels. In particular, we compare the negative buoyancy from liquid water loading (B_l) with the in-cloud virtual

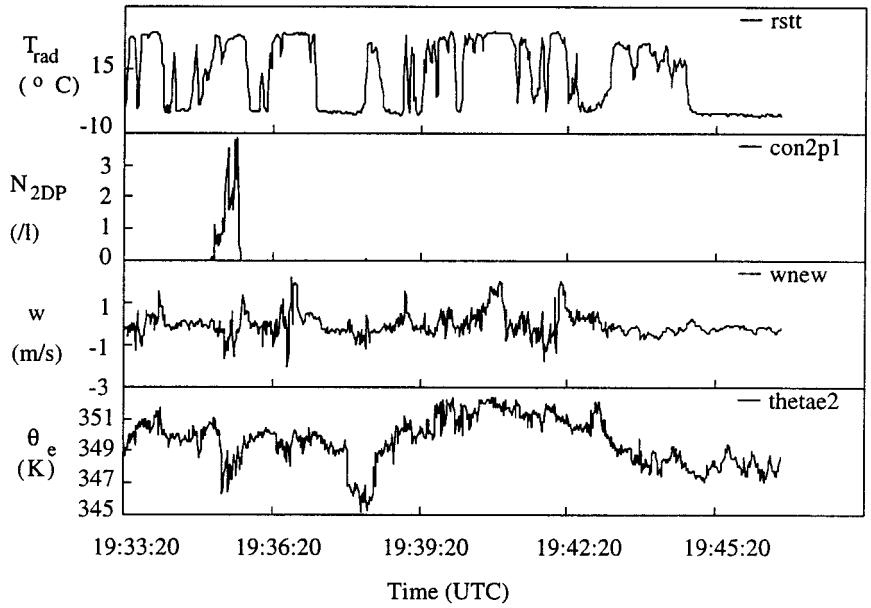

FIG. 3. Data from a leg made at 965 mb on 5 December 1992 beginning at 1933:20 UTC. The panels are from top to bottom: upward radiometer temperature (T_{rad}) in °C; concentration of particles detected by the 2DP, (N_{2DP}) in l; vertical wind velocity, (w) in m s^{-1}; and the reversible equivalent potential temperature, θ_e in K.

temperature excess (ΔT_v) and the difference between the measured ΔT_v and the typical adiabatic ΔT_v. We also illustrate various features of the clouds using data from several penetrations made on 18–19 February 1993.

a. Cloud penetrations from 18–19 February 1993

Eight penetrations were made at three different levels in this cloud system. Figure 4 shows three consecutive penetrations made across a convective line at about 700 mb. The cloud liquid water content is less than 1 g m^{-3} everywhere: with a cloud base of 940.2 mb and temperature of 23.4°C, the adiabatic liquid water content is about 5 g m^{-3}. The precipitation water content q_p is highly variable; as can be seen in the figure, there are narrow regions with large values of q_p adjacent to regions with appreciably lower values. A particularly prominent peak in q_p is associated with a downdraft in Fig. 4a at about 0053 UTC. Here, ΔT_v is positive, but the weight of the precipitation is sufficient to make the value of B in the downdraft negative. This is the so-called warm downdraft (JL). An example of an unusually strong and broad downdraft is seen in Fig. 4c at about 0118 UTC.

There is a 3-km-wide updraft with $w \approx 5$ m s^{-1} at about 0053:30 UTC (Fig. 4a), and a 6-km-wide updraft at about 0105 UTC (Fig. 4b). Both updrafts contain significant precipitation: the maximum value of q_p was about 4.5 g m^{-3} in the later updraft.

There are two regions shown in Fig. 4c where $q_p = 0$ but $q_c > 0$. For example, there is a 1-km-wide updraft at 0118:50 UTC with $w \approx 3$ m s^{-1} and $q_c < 0.75$ g m^{-3}. It is likely that precipitation has fallen out of the parcel, since precipitation is present in other regions of cloud that have similar values of q_c, w, ΔT_v, and B and since q_c is so small. Most of the cloud regions penetrated during TOGA COARE contained precipitation. However, most precipitation-free regions contained very little cloud liquid water: typically $q_c < 1$ g m^{-3}. Indeed only one adiabatic core was measured by the Electra in the entire project (this is shown later in Fig. 7).

b. Buoyancy in updrafts

According to parcel theory, active updrafts that are accelerating upward will have a positive buoyancy and a positive correlation between the vertical velocity and buoyancy. The histogram in Fig. 5 shows that the distributions of ΔT_v and B are skewed toward the positive side with ΔT_v more so. There are several cloud regions with $w > 1$ m s^{-1} and $B < 0$; an example was shown in Fig. 4b. The majority (86%) of 1-s B_l values are smaller than 0.5 K, as Fig. 5 shows.

Figure 6 shows that there is a slight positive correlation between B and w in precipitation-free updrafts that contained more than 0.3 g m^{-3} of cloud liquid water content. There is no correlation when regions containing precipitation are included. Figure 7 shows the time series from a cloud penetration made at 840 mb on 5 December 1992. The aircraft entered the shallow cloud from the southwest and sampled the only adiabatic region in the project. The buoyancy is roughly correlated

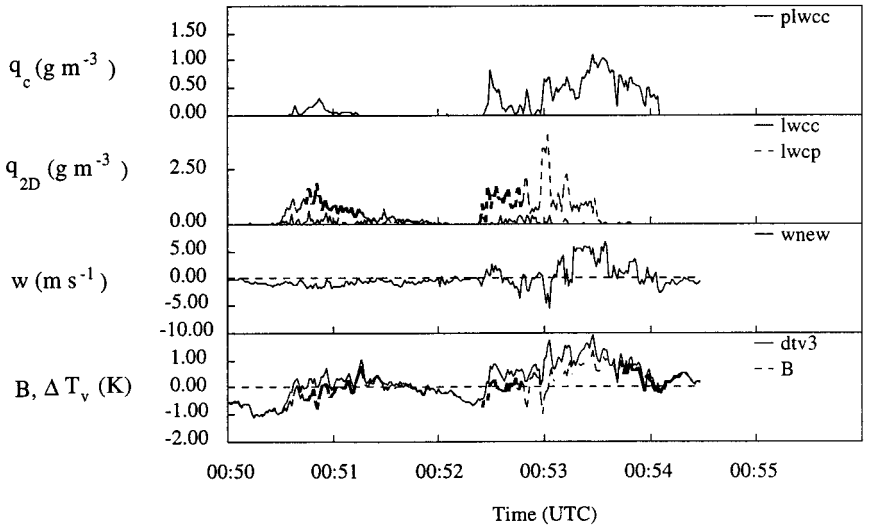

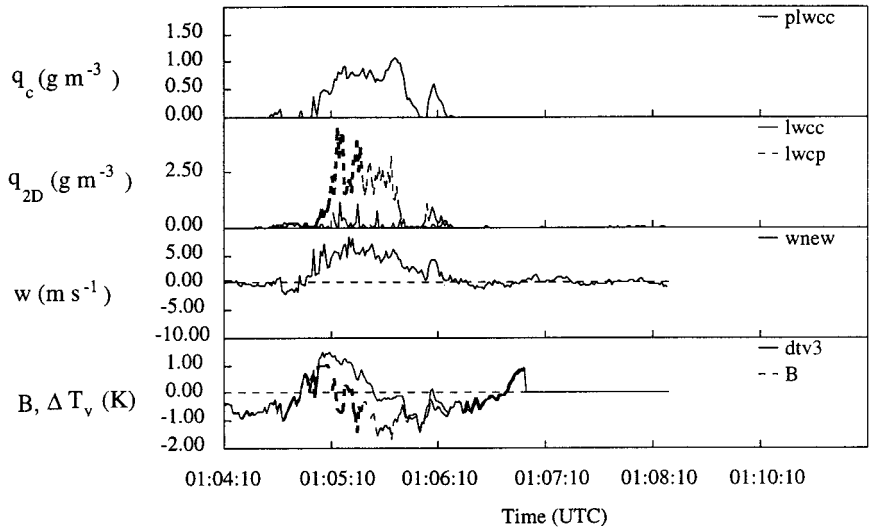

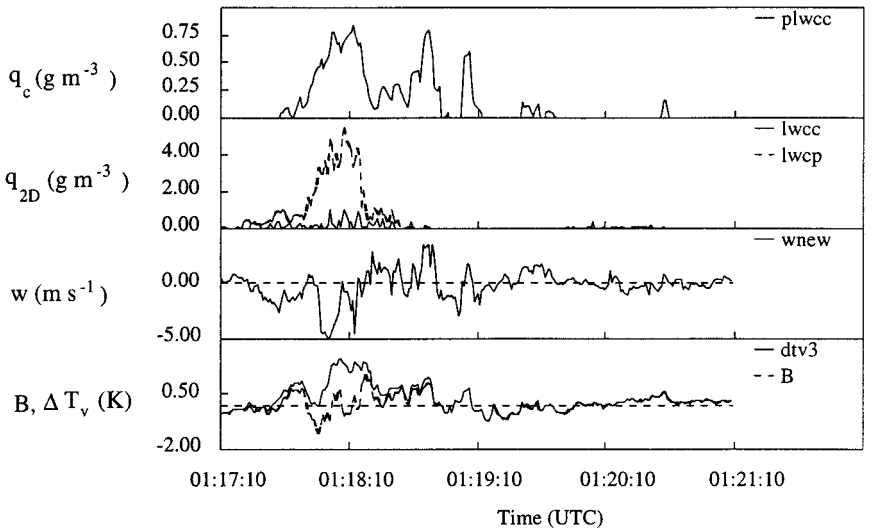

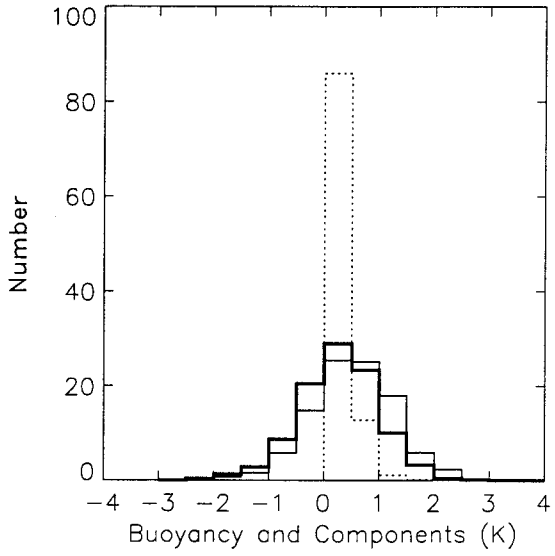

FIG. 5. Histogram of buoyancy B (thick solid line), virtual temperature excess, ΔT_v (thin solid line), and the negative contribution to buoyancy by liquid water loading B_l (dotted line) in all updrafts at all levels with $w > 1$ m s^{-1}.

with vertical velocity during the time period $t = 100 - 130$ s when cloud LWC was high. There is a better correlation between buoyancy and cloud LWC. Four turrets can be distinguished, each with an updraft bounded by weak downdrafts and with a size of 1–2 km. The buoyancy is greatest in the adiabatic core. However, the maximum vertical velocity ($w_{\max} \approx 8$ m s^{-1}) is about the same in the adiabatic core as in two other turrets.

Figure 8 presents the average values of the buoyancy $\overline{B}$, the in-cloud virtual temperature excess $\overline{\Delta T_v}$, and the negative buoyancy due to water loading $\overline{B_l}$ in all updrafts penetrated at the three levels in the 13 flights. The averages are taken over all 1-Hz values in updrafts with $w > 1$ m s^{-1} at each level. It shows that the largest values of $\overline{B}$, $\overline{\Delta T_v}$, and $\overline{B_l}$ in updrafts are at the lowest altitude. The values of $\overline{B}$ are almost equal to $\overline{B_l}$ and about half of $\overline{\Delta T_v}$.

The values of $\overline{\Delta T_v}$ at these three levels are positive. However, they are much lower than the adiabatic values at each level for a typical TOGA COARE sounding. The difference between the typical adiabatic values and the average measured values is larger than 2 K at all three levels. On the other hand, the negative buoyancy resulting from water loading is smaller than 0.4 K. The difference between the adiabatic and measured values increases with altitude as expected from entrainment and mixing theory. The reduction in B due to precipitation water loading (B_l) decreases slightly with height.

Figure 9 shows the variation with the updraft strength of the average values of B, ΔT_v, and B_l taken over all cloud regions with $w > 0$ m s^{-1} at 700 mb. It shows that all three quantities increased with increasing w for $w < 4$ m s^{-1}; they were almost constant for $4 < w < 7$ m s^{-1}, and both $\overline{B}$ and $\overline{\Delta T_v}$ increased rapidly with w for $w > 7$ m s^{-1}, while $\overline{B_l}$ was almost constant. Notice that $\overline{B_l}$ was almost half of the value of $\overline{\Delta T_v}$ for $w < 7$ m s^{-1} but was much less than half when $w > 7$ m s^{-1}. Also, $\overline{B_l} < 0.5$ K for all values of w. On the other hand, the difference between the adiabatic and measured values of $\overline{\Delta T_v}$ was greater than 1.0 K when $w > 7$ m s^{-1} and greater than 2 K when $w < 7$ m s^{-1}, taking the typical adiabatic value of ΔT_v to be 3 K at 700 mb. Therefore, as shown above, the reduction in buoyancy by entrainment in updrafts was much larger than that by precipitation at 700 mb. Furthermore, the reduction by entrainment and mixing decreased with increasing vertical velocity.

c. Buoyancy in downdrafts

As in updrafts, the values of B and ΔT_v in downdrafts approximately followed a normal distribution. However they were slightly skewed to the negative side (Fig. 10). Among the negatively buoyant downdrafts, 17% had positive ΔT_v.

The average values of B, ΔT_v, and B_l taken over all points in downdrafts for the three levels are plotted in Fig. 11. Figures 11a,b are for $w < -1$ m s^{-1} and $w < -3$ m s^{-1}, respectively. The values of $\overline{\Delta T_v}$ in both strong and weak downdrafts were positive at all three levels. Notice $\overline{\Delta T_v}$ increased slightly with height in weak downdrafts (Fig. 11a), while it decreased with height in strong downdrafts (Fig. 11b). Also $\overline{B_l}$ was the largest at the lowest level and approximately the same at the two upper levels in strong downdrafts, and values were about the same at all levels in weak downdrafts. The value of $\overline{B}$ in weak downdrafts is almost zero at the lowest level and slightly positive at the upper levels. Also $\overline{B}$ was larger in stronger downdrafts at the lowest two levels and slightly positive at the upper level. Notice that $\overline{B} > 0$ in downdrafts. Values were less than the average values found in updrafts except at 700 and 850 mb in strong downdrafts (see Figs. 8 and 11). There are a number of points where $\Delta T_v < 0$ and $B < 0$, as can be seen in Fig. 7.

←

FIG. 4. Data from three cloud penetrations made on 19 February 1993 beginning at (a) 0050, (b) 0104:10, and (c) 0117:10 UTC. Note that the flight began on 18 February, so is called the 18 February case. The panels are from top to bottom: cloud liquid water content, q_c, in g m^{-3}, measured by the King probe; precipitation water content measured by the 2DC q_{2DC} (solid line), and the 2DP q_{2DP} (dashed line) both in g m^{-3}; vertical velocity w in m s^{-1}; and ΔT_v (solid line) and B (dashed line) in K. Gaps in the trace of B are due to bad data from the 2D probes.

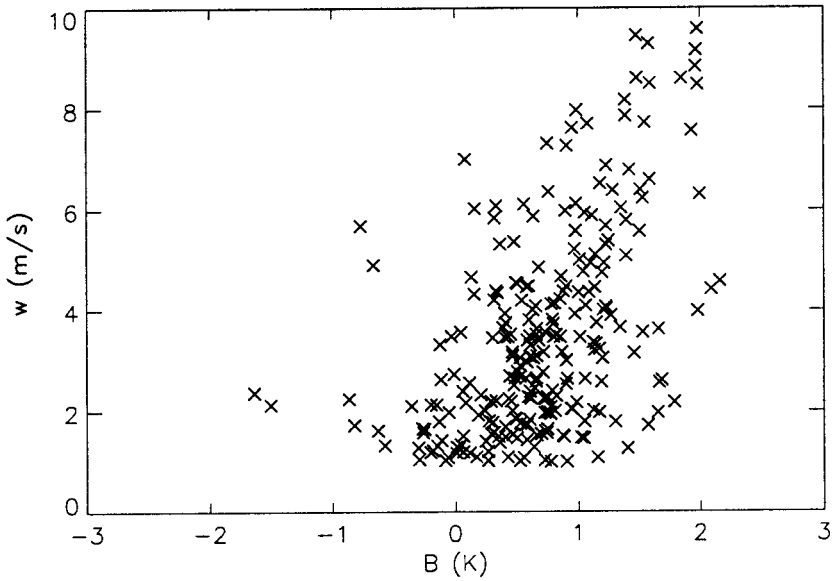

FIG. 6. Scatterplot of w versus B in all updraft regions ($w > 1$ m s^{-1}) at all levels with $q_{2DC} < 0.5$ g m^{-3}, $q_c > 0.3$ g m^{-3} that contained no raindrops with size $D > 800$ μm.

The averages for different vertical velocity intervals in cloud regions with $w < 0$ m s^{-1} at 700 mb are shown in Fig. 12. All values of $\overline{\Delta T_v}$ and $\overline{B}$ are positive and increase with the strength of the downward motion. Here, $\overline{B_l}$ increased as w decreased for $w > -3$ m s^{-1} and remained constant thereafter.

4. Summary and discussion

This paper reports on the buoyancy of TOGA COARE clouds using measurements of temperature made with the Ophir radiometer, and cloud and precipitation water loading measured by the King and John-

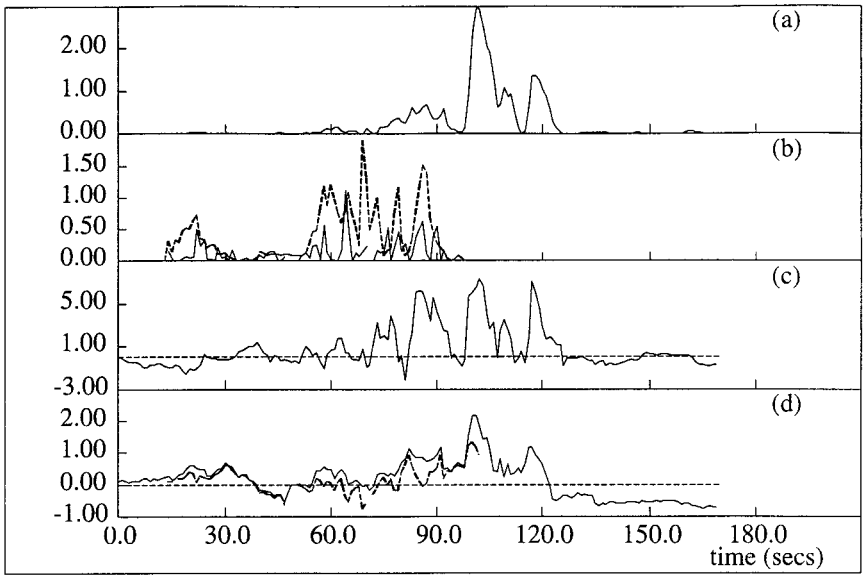

FIG. 7. Data taken from the cloud penetration starting at 840 mb at 2011:40 UTC 5 December 1992. Panels are from top to bottom: (a) cloud liquid water content q_c measured by the Johnson–Williams probe in g m^{-3}; (b) precipitation water content from 2DC q_{2DC} (solid line) and 2DP q_{2DP} (dashed line) in g m^{-3}; (c) vertical air velocity w in m s^{-1}; and (d) virtual temperature excess ΔT_v (solid line) and buoyancy B (dashed line) in K. The adiabatic values of cloud liquid water content and buoyancy are 3 g m^{-3} and about 1.3 K, respectively, at this level.

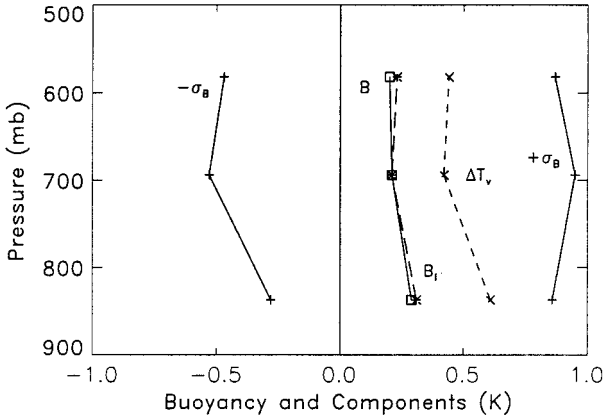

FIG. 8. Averages taken in updrafts with $w > 1$ m s^{-1} of B (□ joined by solid line), ΔT_v (× joined by short dashed line), and B_l (* joined by long dashed line) plotted versus pressure P. The standard deviation for B, $\pm\sigma_B$ is shown by + joined by a solid line. The number of samples at each level are 704 at 850 mb; 2748 at 700 mb; and 166 at 600 mb.

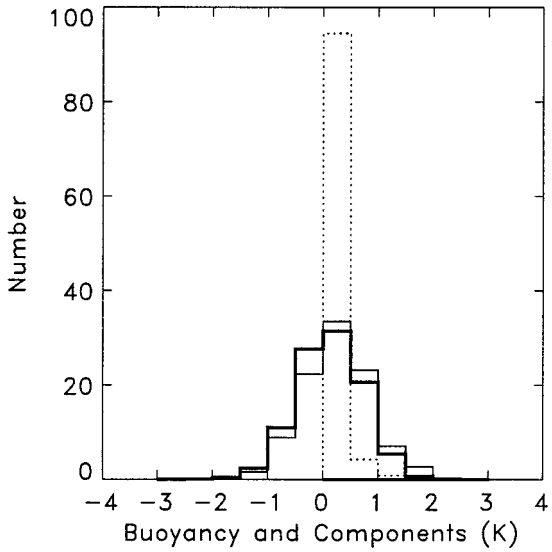

FIG. 10. Same as Fig. 5, but for downdrafts ($w < -1$ m s^{-1}).

son–Williams probes and PMS probes. The most significant results are summarized below.

- The reduction in buoyancy due to the reduction of the virtual temperature excess by entrainment from the adiabatic value is much greater than the negative contribution to buoyancy due to precipitation on average.
- Precipitation water content is highly variable both during a penetration and from one penetration to the next (e.g., see Fig. 4). Also, there are several cloud regions where $B_l = 0$, $B > 0$, $w > 5$ m s^{-1}, but the cloud liquid water content is very low (e.g., Fig. 4). These observations suggest that precipitation only temporarily slows a parcel down: once the precipitation has fallen out, the parcel accelerates upward. This and the previous result show that entrainment and mixing play a much larger role in reducing the buoyancy than precipitation loading.
- The average buoyancy in downdrafts is positive and is similar to the value in updrafts at all levels (see Figs. 8 and 11). The result suggests that downdrafts are transient.
- The cloud liquid water content is usually less than 0.1 of the adiabatic value even in updrafts. Such low values are most likely caused by conversion of cloud water to precipitation.
- The average value of ΔT_v in updrafts increases with

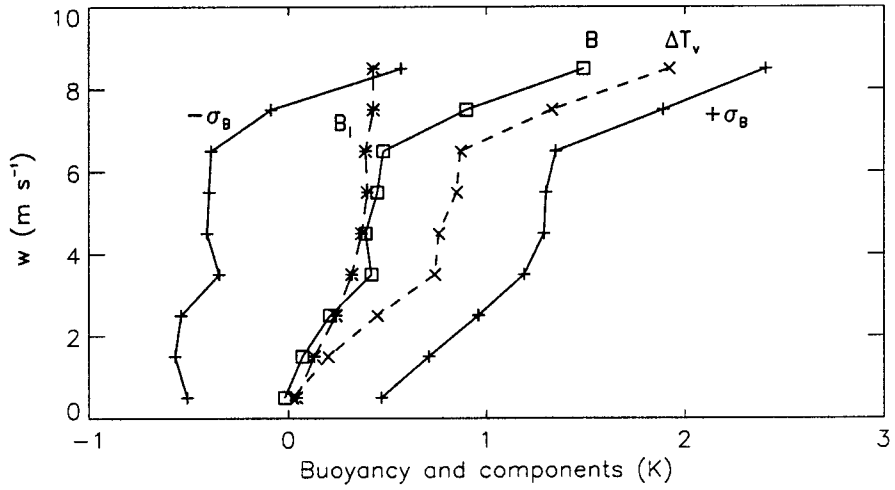

FIG. 9. Averages taken over 1 m s^{-1} intervals in cloud regions with $w > 0$ m s^{-1} at 700 mb of B (□ joined by solid line), ΔT_v (× joined by short dashed line), and B_l (* joined by long dashed line) plotted versus w. The standard deviation for B, $\pm\sigma_B$ is shown by + joined by a solid line. There were over 100 samples with $w < 6$ m s^{-1}, but there were only 73, 32, and 15 samples for $7 > w > 6$ m s^{-1}, $8 > w > 7$ m s^{-1} and $8 > w > 9$ m s^{-1}, respectively.

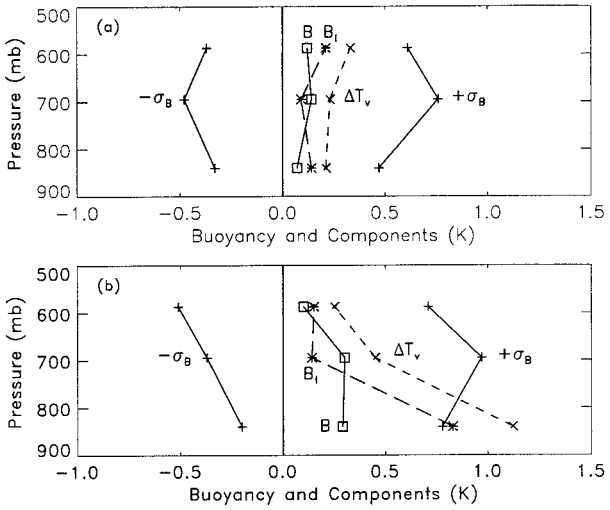

FIG. 11. Same as Fig. 8, but for (a) all downdrafts with $w < -1$ m s^{-1}, and (b) strong downdrafts with $w < -3$ m s^{-1}. The number of samples at each level are for (a) 933 at 850 mb, 3149 at 700 mb, and 760 at about 600 mb, and for (b); 28 at 850 mb, 176 at 700 mb, and 11 at about 600 mb.

w (Fig. 9) indicating that updrafts which have been affected less by entrainment and mixing are more vigorous, as expected. The average of B_l also increases with w, although less rapidly. This is probably because more cloud liquid water is available for the precipitation process with less entrainment and mixing.

It is clear that on average the effects of entrainment and mixing are much greater than precipitation in reducing the buoyancy in TOGA COARE clouds. Typically the available buoyancy is about 2–3 K at 700 mb, the reduction of ΔT_V due to entrainment is about 2 K, while the negative buoyancy due to the weight of precipitation is typically less than 0.5 K. However, we must be careful to place the conclusions in the context of how the measurements were made. Only one adiabatic core was measured during the project: it is likely that many more existed at 850 mb, but were missed because of the flight strategies. Even though adiabatic cores may be elusive in an average sense, their role in influencing the dynamics and microphysics should not be overlooked. For example, the influence of precipitation loading is possibly much larger than that of entrainment in reducing the buoyancy in near-adiabatic cores. Further field experiments are needed to specifically examine adiabatic cores in tropical clouds.

Negatively buoyant warm downdrafts, such as were observed by JL, LZL, and others, were also often observed in these TOGA COARE clouds. However, a surprising result from this study is that on average, downdrafts were found to be positively buoyant. Igau et al. (1998, manuscript submitted to *J. Atmos. Sci.*) and M. A. LeMone (1998, personal communication) suggest that some of the positively buoyant downdrafts may in fact be negatively buoyant if downdrafts are not saturated as assumed. They examined several of the strongest downdrafts and concluded that a few of them could in fact be negatively buoyant if the relative humidity in the downdraft was lower than 80%. However, they found that even if the relative humidity in downdrafts was 60% (which is less than the average environmental value) rather than the assumed 100%, there would still be many positively buoyant downdrafts. Downdrafts are usually negatively buoyant due to evaporation in cumulus clouds over the High Plains of the United States (e.g., Blyth et al. 1988) and models using only buoyancy have been relatively successful in describing the source of entrained air and horizontal divergence in these clouds (e.g., Raymond and Blyth 1986, 1992).

The results reported herein suggest that more detailed models will be required to describe clouds that form in the moister environments over the tropical oceans. Fi-

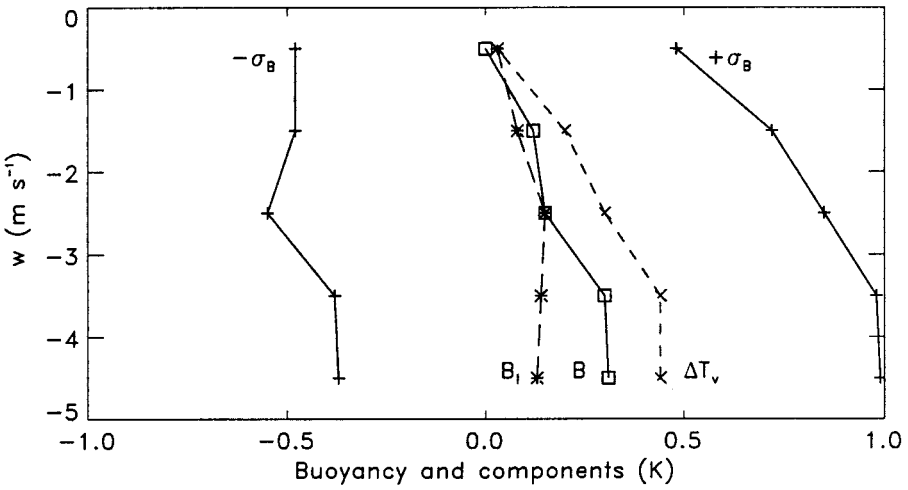

FIG. 12. Same as Fig. 9, but for cloud regions with $w < 0$ m s^{-1} at 700 mb. There were over 2500 1-Hz samples for intervals with $w > -4$ m s^{-1} but only 33 with $-5 < w < -4$ m s^{-1}.

nally, it is clear that improvements should continue to be made in measuring in-cloud temperature, humidity, and cloud liquid water content, particularly in the individual turrets of tropical cumulus clouds.

Acknowledgments. We are grateful to the many people involved in TOGA COARE, especially the people at NCAR responsible for operating the Electra and the data produced. We are also grateful to Peggy LeMone for providing video tapes and for many discussions, Paul Lawson for advice on using the Ophir, and to Ed Zipser and Rick Igau for their contribution to the work. We also thank Peggy LeMone, Ed Zipser, and an anonymous reviewer for helping to improve the manuscript through their careful reviews. This work was supported by the National Science Foundation Grant ATM-9413289 and the TOGA COARE Grant ATM-9112043.

REFERENCES

Albrecht, B. A., S. K. Cox, and W. H. Schubert, 1979: Radiometric measurements of in-cloud temperature fluctuations. *J. Appl. Meteor.,* **18,** 1066–1071.

Barnes, G. M., E. J. Zipser, D. P. Jorgensen, and F. D. Markes Jr., 1983: Mesoscale and convective scale structure of a hurricane rainband. *J. Atmos. Sci.,* **40,** 2125–2137.

Baumgardner, D., 1989: Airborne measurements for cloud microphysics. NCAR Research Aviation Facility Bulletin No. 24, 22 pp. [Available from NCAR, P.O. Box 3000, Boulder, CO 80307.]

Beard, K. V., 1983: Reorientation of hydrometeors in aircraft accelerated flow. *J. Appl. Meteor.,* **22,** 1961–1963.

——, and A. R. Jameson, 1983: Raindrop canting. *J. Atmos. Sci.,* **40,** 448–454.

Blyth, A. M., W. A. Cooper, and J. B. Jensen, 1988: A study of the source of entrained air in Montana cumuli. *J. Atmos. Sci.,* **45,** 3944–3964.

Byers, H. R., and R. R. Braham, 1949: The Thunderstorm Project. U.S. Weather Bureau, U.S. Dept. of Commerce Tech. Rep., 287 pp. [NTIS PB234515.]

Chandrasekar, V., W. A. Cooper, and V. N. Bringi, 1988: Axis ratios and oscillations of raindrops. *J. Atmos. Sci.,* **45,** 1323–1333.

Cooper, W. A., 1987, The Ophir radiometric thermometer: Preliminary evaluation. NCAR Tech. Note NCAR/TN-292+STR, 54 pp. [Available from NCAR, P.O. Box 3000, Boulder, CO 80307.]

——, V. N. Bringi, V. Chandrasekar, and T. Seliga, 1983: Analysis of raindrop parameters using a 2-D precipitation probe with application to differential reflectivity. Preprints, *21st Conf. on Radar Meteorology,* Boston, MA, Amer. Meteor. Soc., 488–493.

Heymsfield, A. J., and J. L. Parrish, 1979: Techniques employed in the processing of particle size spectra and state parameter data obtained with T-28 aircraft platform. NCAR Tech. Note NCAR/TN-134+1A, 78 pp. [Available from NCAR, P.O. Box 3000, Boulder, CO 80307.]

——, J. E. Dye, and C. J. Biter, 1979: Overestimates of entrainment from wetting of the aircraft temperature sensors in cloud. *J. Appl. Meteor.,* **18,** 92–95.

Jorgensen, D. P., and M. A. LeMone, 1989: Vertical velocity characteristics of oceanic convection. *J. Atmos. Sci.,* **46,** 621–640.

——, E. J. Zipser, and M. A. LeMone, 1985: Vertical motions in intense hurricanes. *J. Atmos. Sci.,* **42,** 839–856.

Knollenberg, R. G., 1981: Techniques for probing cloud microstructure. *Clouds, Their Formation, Optical Properties and Effects,* P. V. Hobbs and A. Deepak, Eds., Academic Press, 15–89.

Lawson, R. P., 1990: Thermodynamic analysis of buoyancy and entrainment in cumuli using measurements from a radiometric thermometer. Preprints, *Conf. on Cloud Physics,* San Francisco, CA, Amer. Meteor. Soc., 685–692.

——, and A. Rodi, 1987: Airborne tests of sensor wetting in a reverse flow temperature probe. Preprints, *Sixth Symp. on Meteorology Observations and Instrumentation,* New Orleans, LA, Amer. Meteor. Soc., 253–256.

——, and W. A. Cooper, 1990: Performance of some airborne thermometers in cloud. *J. Atmos. Oceanic Technol.,* **7,** 480–494.

LeMone, M. A., 1980: On the difficulty of measuring temperature and humidity in cloud: Comments on shallow convection on day 261 of GATE. *Mon. Wea. Rev.,* **108,** 1702–1707.

——, and E. J. Zipser, 1980: Cumulonimbus vertical velocity events in GATE. Part I: Diameter, intensity and mass flux. *J. Atmos. Sci.,* **37,** 2444–2457.

Lenschow, D. H., and W. T. Pennell, 1974: On the measurement of of in-cloud and wet-bulb temperatures from an aircraft. *Mon. Wea. Rev.,* **102,** 447–454.

Lucas, C., E. J. Zipser, and M. A. LeMone, 1994a: Vertical velocity in oceanic convection off tropical Australia. *J. Atmos. Sci.,* **51,** 3183–3193.

——, ——, and ——, 1994b: Convective available potential energy in the environment of oceanic and continental clouds: Correction and comments. *J. Atmos. Sci.,* **51,** 3829–3930.

Magono, C., 1954: On the shape of water drops falling in stagnant air. *J. Meteor.,* **11,** 77–79.

Politovich, M. K., and W. A. Cooper, 1988: Variability of the supersaturation in cumulus clouds. *J. Atmos. Sci.,* **45,** 1651–1664.

Pruppacher, H. R., and K. V. Beard, 1970: A wind tunnel investigation of the internal circulation and shape of water drops falling at terminal velocity in air. *Quart. J. Roy. Meteor. Soc.,* **96,** 247–256.

Raymond, D. J., 1995: Regulation of moist convection over the west Pacific warm pool. *J. Atmos. Sci.,* **52,** 3945–3959.

——, and A. M. Blyth, 1986: A stochastic mixing model for nonprecipitating cumulus clouds. *J. Atmos. Sci.,* **43,** 2708–2718.

——, and ——, 1992: Extension of the stochastic mixing model to cumulonimbus clouds. *J. Atmos. Sci.,* **49,** 1968–1983.

Webster, P. J., and R. Lucas, 1992: TOGA COARE: The Coupled Ocean–Atmosphere Response Experiment. *Bull. Amer. Meteor. Soc.,* **73,** 1377–1416.

Zipser, E. J., and M. A. LeMone, 1980: Cumulonibus vertical velocity events in GATE, Part II: Synthesis and model core structure. *J. Atmos. Sci.,* **37,** 2458–2469.